Dalton Transactions

Accepted Manuscript

ROYAL SOCIETY OF CHEMISTRY

www.rsc.org/dalton

Custom designed nanocrystalline Li_2MSiO_4/reduced graphene oxide (M=Fe, Mn) formulations as high capacity cathodes for rechargeable lithium batteries

D. Bhuvaneswari[a], N. Kalaiselvi[*a]

[a]- ECPS Division, CSIR-Central Electrochemical Research Institute, Karaikudi-630006, India.

Abstract: Nanocrystalline Li_2MSiO_4 (M=Fe, Mn) particles embedded between in-situ formed rGO sheets are obtained by adopting customized solvothermal synthesis. An appreciable room temperature specific capacity of 149 mAh g^{-1} with 89% capacity retention and 210 mAh g^{-1} with 87% retention have been exhibited by Li_2FeSiO_4/rGO and Li_2MnSiO_4/rGO composites, corresponding to the participation of close to one and more than one lithium per formula unit respectively. Formation of nanocrystalline Li_2MSiO_4 (M= Fe, Mn) compounds in the desired phase and the complete wrapping of orthosilicates with rGO sheets are believed to be responsible for the excellent electrochemical behavior of orthosilicate cathodes of the present study to best suit with requirements of rechargeable lithium-ion batteries. The abundant availability and eco-benignity advantages of Fe and Mn offer value addition to consider Li_2MSiO_4/rGO (M= Fe, Mn) cathodes as sustainable potential candidates.

Keywords: Lithium-ion battery, nanocrystalline, composite, charge transfer, capacity

Fax: +91 04565-227779
E-mail: kalaiselvicecri@gmail.com

1. Introduction

Lithium-ion battery (LIB) is a key technology to address global energy requirements and has been looking towards greener and sustainable electrodes. Among the two classes of potential lithium intercalating electrode materials, viz., oxide cathodes with an anion close-packed or almost close-packed lattice and polyanionic $(XO_4)^{n-}$ materials, presence of oxide frame work poses intrinsic safety problems due to the release of oxygen into the electrolyte, and causes fire hazard.[1] On the other hand, polyanion structures such as phosphates, silicates, sulfates and borates offer much improved safety because of the covalent nature of oxygen bonding, which in turn prevents the release of oxygen and ensures stability also.[2, 3]Besides safety and excellent electrochemical behavior, recommendation on the feasibility and economic viability of lithium intercalating cathode candidates for practical applications in rechargeable lithium batteries is critically important, thus emphasizing more concern on the availability of raw materials. It is in this connection, the title composites assume importance as sustainable electrodes by considering the abundant availability of raw materials and the additional benefits arising from the eco-benign nature of iron and manganese based electrode materials.

Orthosilicates with a general formula of Li_2MSiO_4 (M = Fe, Mn, Co, Ni) offer the possibility of reversibly extracting/inserting two lithium ions per formula unit with a theoretical capacity of ~330 mAh g^{-1}, thus gaining significant importance. Despite the possibility of realizing a two electron red-ox process involving both M^{2+}/M^{3+} and M^{3+}/M^{4+} red-ox couples,[4-8]most of the literature reports are available on the computational findings and on structure-property relationship,[6-8] leaving behind limited results on the electrochemical performance. The less studied electrochemical properties of orthosilicates could be understood from the view point of difficulty in synthesizing the product in the desired phase, driven primarily by the

polymorphism of Li_2MSiO_4 family compounds.[9] These cathodes also suffer from poor electronic conductivity (~6×10^{-14} S cm^{-1}), which is three times lower than that of olivine $LiFePO_4$.[10] In addition, extraction of two lithium per formula unit is practically limited due to structural instability and higher lithium-ion diffusion barrier (0.9 eV) of Li_2MSiO_4 compared with that of $LiFePO_4$ (0.6 eV).[11]

Of the orthosilicates, Li_2FeSiO_4 and Li_2MnSiO_4 with an orthorhombic structure (based on β-Li_3PO_4) and *Pmn21* space group[12] have been chosen for the study for reasons of economic and environmental benefits and focus was given to custom design a composite structure, suitable for high capacity lithium battery applications. Among the two silicates, Li_2FeSiO_4 has been reported to exhibit 160 mAh g^{-1} at low current density and under high temperature conditions.[13] On the other hand, Li_2MnSiO_4 cathode with an inferior electronic conductivity than Li_2FeSiO_4 at a given temperature, offers the possibility of reinsertion of more than 1.5 lithium to exhibit ~200 mAh g^{-1} at room temperature and 250 mAh g^{-1} at 50 °C, provided reduced particle size and carefully chosen conductive carbon additive are taken into consideration[13-16]. With regard to orthosilicates, conventional carbon additives are not suitable to overcome the extremely poor electronic conductivity of them. On the other hand, preparation of carbon rich composite with a post heat treatment results in the formation of carbon lumps that leads to sluggish lithium-ion transport. Therefore, formation of silicate composites with a suitable carbon additive, wherein combination of carbon coating or wrapping of cathode active material with a desired thickness of carbon coating that facilitates continuous wiring of individual silicate particles to improve the electronic conductivity and lithium diffusion kinetics of the electrode poses challenges.

It is well known that graphene; by virtue of the presence of sp^2 bonded carbon atoms arranged in hexagonal 2D lattice would offer high electronic conductivity[17]. Considering the

high surface/mass ratio and the inherent high electronic conductivity, it is believed that graphene would offer thin carbon coating and hence problems due to more carbon loading could be avoided. Based on these reasons, reduced graphene has been chosen to form the composite of silicate cathodes of the present study. The most popular approach of reducing the exfoliated graphene oxide (GO) obtained by Hummer's method[18] has been adopted to prepare rGO or simple graphene. Basically, reduction of GO results in the partial restoration of electrical conductivity and the material thus obtained viz., rGO has been used to wrap Li_2MSiO_4 particles to form Li_2MSiO_4/rGO composite, which is the prime objective of the study. Such a wrapping of orthosilicate with reduced graphene oxide is expected to enhance the electronic transport[19,20] vis-a-vis the ultimate electrochemical properties of rGO wrapped Li_2FeSiO_4 and Li_2MnSiO_4 cathodes individually, thus leading to the possibility of exploiting custom designed Li_2MnSiO_4/rGO composites as high capacity cathodes for rechargeable lithium battery.

Li_2MSiO_4 (M= Fe, Mn) samples were prepared by low temperature solvothermal synthesis method to avoid side reactions and phase separation[21]. The synergistic advantage of formation of orthosilicates in the desired phase and the conducting effect of rGO in facilitating facile lithium intercalation and de-intercalation behavior of Li_2MSiO_4/rGO composite cathodes has been discussed.

2. Experimental Section

***2.1. Synthesis*:** LiOH. H_2O (Aldrich) was added to SiO_2 (Aldrich) dispersed in 20 ml of distilled water and stirred. Manganese acetate and $FeCl_2$ (Aldrich) were added individually to 10 ml of tri ethylene glycol (TEG) solvent and stirred with gentle heating until dissolution occurred. The precursors were taken in the ratio 2:1:1. The aforesaid solutions were mixed with stirring and the slurry thus obtained was transferred to a (20 ml) of in-house made Quartz container and sealed in

an autoclave. The sealed autoclave was heated at 300 °C for 24h for the complete transformation of precursors into orthosilicates. The product was filtered and dried overnight at 80 °C. The as-prepared nanocrystalline Li_2MSiO_4 has been added during the preparation of rGO prior to the reduction step, in order to obtain in-situ formed Li_2MSiO_4/rGO composite.

2. 2. Structural and Chemical Characterization: X-ray diffraction (XRD) characterization of the samples was carried out with a Philips X'Pert diffractometer using Cu Kα radiation. Field emission scanning electron microscopy (FESEM) and transmission electron microscopy (TEM) characterizations were carried out respectively with JEOL-JSM5610 SEM and JEOL JEM-2010F equipments. Raman spectroscopic analysis was performed with a Renishaw InVia system utilizing a 514.5 nm incident radiation. Thermogravimetry and differential thermal analysis (TG/DTA) were recorded with a thermo balance model STA 409 PC in the temperature range 25–800 °C, using alumina crucibles, under air with a heating rate of 20 °C/min.

2. 3. Electrochemical Characterization: Electrochemical performance of Li_2MSiO_4/rGO has been evaluated in CR 2032 coin cells. Cathode was prepared from a combination of 70 wt% active material (Li_2MSiO_4/rGO) with 20 wt% super P conductive carbon and 10 wt% poly vinylidene fluoride (PVdF) binder. The coin cell fabrication was carried out in an argon-filled glove box using Li_2MSiO_4/rGO cathode, metallic lithium anode, 1 M $LiPF_6$ in 1:1 diethyl carbonate/ethylene carbonate electrolyte and Celgard separator. Cyclic voltammetry (CV) was performed using an Autolab electrochemical work station and charge- discharge studies were carried out using ARBIN charge-discharge cycler. Electrochemical impedance spectroscopy (EIS) measurements were carried out using a VMP3 (Bio-Logic Science Instruments) tester and the experimental data were analyzed using EC-Lab V10.19 software. The conductivity value was measured using LCR conductivity meter.

3. Results and Discussion

Fig. 1a and b show the powder X-ray diffraction pattern of as-synthesized Li_2FeSiO_4/rGO and Li_2MnSiO_4/rGO samples. The recorded XRD pattern exhibits well resolved peaks, thereby indicating the crystalline nature of as-synthesized Li_2MSiO_4/rGO (M=Fe, Mn) composites. The XRD pattern of Li_2FeSiO_4 confirms the presence of monoclinic phase with $P2_1$ space group. No diffraction peaks due to unreacted starting materials or Fe_3O_4 and Li_2SiO_3 impurity phases are seen in the final product. On the other hand, the crystal structure of the Li_2MnSiO_4 sample has been identified as an orthorhombic phase with a $Pmn2_1$ space group. Interestingly, the Bragg pattern of Li_2MnSiO_4 consists of no peaks corresponding to the presence of MnO and Mn_2SiO_3, with an exception of few low-intensity Li_2SiO_3 peaks. Upon comparison, the Li_2FeSiO_4 and Li_2MnSiO_4 synthesized by citric acid assisted sol-gel method contain (Fig. S1) high intensity impurity peaks due to Fe_2O_3, MnO and $MnSiO_4$ along with Li_2SiO_3, thus substantiating the superiority and suitability of solvothermal method to prepare Li_2MSiO_4 (M= Fe, Mn) compound, with the desired purity. The total carbon content of Li_2MSiO_4/rGO composites, calculated from TG-DTA (Fig. S2) is found to be around 4-5 wt%.

Morphological features of solvothermally synthesized Li_2MSiO_4/rGO (M= Fe, Mn) are furnished in Fig. S3. Herein, the SEM images of as synthesized Li_2FeSiO_4 and Li_2MnSiO_4 consist of particles in the range of 100 nm without agglomeration. On the other hand, sol-gel synthesized Li_2MSiO_4 (M=Fe and Mn) samples (Fig. S4) depict the presence of coarsened particles of around 500 nm size. FESEM images of solvothermally synthesized Li_2FeSiO_4/rGO and Li_2MnSiO_4/rGO composite are shown in Fig. 2a-d. Formation of nanocomposite with rGO is evident, especially from FESEM images, where the wrinkled appearance of the reduced graphene oxide layers is distinguishable from the particles of pristine Li_2MSiO_4 (M= Fe, Mn)

cathode materials. Elemental mapping results are shown in Fig. S5. These results indicate the presence of Fe/Mn, Si, and O elements, proving the formation of desired lithium metal silicates with homogeneous distribution. TEM images of solvothermally synthesized (Fig. S6a and b) Li_2MSiO_4 (M= Fe) exhibit non-aggregated spherical particles of 50–100 nm, which is comparable with the results of SEM study. The corresponding composites obtained with the addition of 10 wt% super P carbon (Fig. S6 c-d) and CNT (Fig. S6 e-f) also evidence the growth controlled particles of Li_2MSiO_4 (M=Fe, Mn), which are encapsulated with the added carbon.

TEM images of currently synthesized rGO (Fig. 3a and b) show the presence of transparent graphene sheets. The SAED pattern (Fig. 3a Inset) indicates the perfect hexagonal arrangement of carbon spotting, thus confirming the presence of crystalline rGO containing orderly arranged layers. Interestingly, the TEM images (Fig. 3c-f) evidence the presence of Li_2MSiO_4 (M= Fe, Mn) composites, which are completely wrapped by rGO sheets. The closer view of rGO wrapped silicates is seen in Fig. S7 a-d, wherein Fig. S7 b apparently depicts the presence of silicate particles encapsulated by the transparent rGO sheets. Further, SAED pattern of Li_2MSiO_4/rGO composites show cloudy ring pattern (Fig. 3 Inset), thus confirming the sheet like attachment of rGO[22], as understood already from FESEM results. On the other hand, the TEM images of Li_2MSiO_4 (M=Fe, Mn) super P carbon composites are shown in Fig. S7 c and d, wherein, formation of carbon lump is clearly seen, which in turn may limit the lithium diffusion kinetics.

FTIR spectra (Fig. S8) recorded for as-synthesized Li_2FeSiO_4 and Li_2MnSiO_4 show significant absorption bands around 900 cm^{-1}, corresponding to the presence of O–Si–O stretching vibration and the other band around 730 cm^{-1} may be correlated to the presence of $(SiO_3)^{2-}$ group.[23] Unlike pristine graphite that displays a strong G band sat 1571 cm^{-1} and a weak

D band at 1352 cm^{-1}, Raman spectrum of the currently synthesized GO and rGO (Fig. S9 a and b) shows a broadened G band and an intense D band around 1570 and 1350 cm^{-1} respectively. This is an indication of possible decrease in the size of the in-plane sp^2 domains and enhanced conjugation of the structure,[24] resulting from the extensive oxidation and ultrasonic exfoliation. The same could be further understood from the calculated I_D/I_G ratio of 1.55 (Fig. S9 b), which is higher than the reported results.[25] Raman spectra of in-situ formed Li_2MSiO_4/rGO composites (Fig. 4a and b) confirm the attachment of cathode active material and rGO sheets, as evident from the characteristic peak broadening, position and pattern of peaks.

The electrochemical behavior of Li_2MSiO_4/rGO (M=Fe, Mn) composite cathodes has been investigated by cyclic voltammetry in a wide potential window of 2.0-4.9 V (Fig. 5) and at a slow scan rate of 0.1 m V s^{-1}. In both the cases, first CV cycle corresponds to the irreversible surface reactions of formation cycle and the same has not appeared in further cycles, which is an acceptable behavior. In the case of Li_2FeSiO_4/rGO cathode (Fig. 5a), red-ox peak pairs observed at 3.3 and at 2.5 V during the first cycle correspond to the one step oxidation and reduction related to Fe^{2+}/Fe^{3+} couple.[26] Herein, a possible second lithium extraction corresponding to Fe^{3+}/Fe^{4+} red-ox couple is not observable. Further, a slight shift in the cathodic peak upon progressive cycling that appears at 2.5 V in the reverse scan may be correlated to structural rearrangements[26,27] which is in agreement with the reported results. On the other hand, the cyclic voltammogram of Li_2MnSiO_4/rGO (Fig. 5b) is quite interesting. It shows a red-ox peak at 4.1/3.3 V, corresponding to Mn^{2+}/Mn^{3+} couple and the second red-ox peak at 4.7/4.33 is due to Mn^{3+}/Mn^{4+} redox couple.[28] During the second cycle, the oxidation peak is shifted and a broad peak appears at ~4.7 V, which upon further cycling resumes the two stage red-ox behavior of the first cycle. Fig. 5c and d show the CV behavior of Li_2MSiO_4/C (M=Fe, Mn) composite cathodes

with 10 wt% CNT carbon. Herein, despite the appearance of oxidation and reduction peaks at the respective positions, the reduction peaks is not pronounced, which is noteworthy.

Galvanostatic charge-discharge studies were carried out at a moderate rate of C/20 between 2.5 and 4.9 V to evaluate the lithium intercalating capability of synthesized cathodes. Generally, the insertion/de-insertion potential are about 3.2 and 4.7 V for Li_2FeSiO_4 and about 4.1 and 4.5 V for Li_2MnSiO_4.[27] Further, it is well known that the discharge behavior depends on the crystallinity of cathode active material and the type of conducting matrix present in the cathode composition. In order to demonstrate the same and to understand further, composites of Li_2MSiO_4/C (M=Fe, Mn) have been prepared with super P carbon selected based on our earlier and on-going research on similar compounds and subjected to charge-discharge studies. Fig. S10 a-d shows the first and second charge-discharge profile of Li_2MnSiO_4/C and Li_2FeSiO_4/C cathodes, wherein, poor reversible capacity is observed in the second cycle for both the cathodes, along with a drastic capacity fade, exhibited upon progressive cycling. Henceforth, composites of other carbon sources like CNT and rGO mixed with Li_2MSiO_4 electrodes have been chosen for the present study. Herein, we found a negligible difference in polarization and better capacity retention behavior (Fig. 6a and c) due to the preserved conductive network upon extended cycles. However, presence of slope like profile is evident from the figure, which is not uncommon, because similar electrochemical intercalation/deintercalation behavior has been reported for silicate cathodes, especially with high surface area than the bulk particles [1, 3]. The charge-discharge results of super P carbon composite of Li_2MnSiO_4/C and Li_2FeSiO_4/C cathodes are furnished in the supplementary document as Fig. S10. In other words, Li_2MSiO_4/C (M=Fe, Mn) composites with CNT (10 wt%) were subjected to charge-discharge studies, wherein, an inferior reversible capacity of about 110 mAh g^{-1} and a rapidly reducing discharge capacity behavior

from 250 to 110 mAh g^{-1} have been observed for Li_2FeSiO_4/CNT and Li_2MnSiO_4/CNT cathodes respectively (Fig. 6a and b) at C/20 rate. On the other hand, Li_2FeSiO_4/rGO composite cathode delivers (Fig. 6c) an appreciable initial discharge capacity of 215 mAh g^{-1} and Li_2MnSiO_4/rGO to the extent of 234 mAh g^{-1} (Fig. 6d), thereby demonstrating the superiority of rGO over CNT as a conductive carbon additive and as a composite matrix in facilitating facile lithium intercalation behavior of pristine Li_2MSiO_4 (M=Fe, Mn) cathodes. Particularly, Li_2FeSiO_4/rGO composite cathode upon progressive cycling exhibits a significant change in the working potential itself, which is not unusual (Fig. 6c). Interestingly, the magnitude of specific capacity observed with Li_2FeSiO_4/rGO cathode and the shift in plateau position corresponds to a possible involvement of more than one lithium ion in the intercalation/de-intercalation process and the unavoidable structural rearrangements associated especially with orthosilicate cathodes involving the participation of more than one lithium per formula unit. In other words, upon such extraction, some of Li^+ ions in the 4b site and Fe ions in the 2a site are interchanged to stabilize the structure.[28] This has been reflected in the larger irreversibility of about 64 and 48 mAh g^{-1} observed during first two cycles. However, a stable charge/discharge capacity of about 149 mAh g^{-1} up to 100 cycles (Fig. 7) has been exhibited by Li_2FeSiO_4/rGO with 89% retention, which may be attributed to the extraction of one lithium per formula unit without involving any structural change upon extended cycling. Such a behavior of more than one lithium extraction during few of the initial cycles and the subsequently restricted participation of one lithium per formula unit upon continuous cycling is also in agreement with the reported results[29] However, extraction of 149 mAh g^{-1} from Li_2FeSiO_4/rGO at C/20 rate and cycleability at room temperature operating condition is superior than most of the reported results[30] and the same is the significance of the present work.

Further to our interest, Li_2MnSiO_4/rGO cathode exhibits (Fig. 6d) the highest first charge capacity of 310 mA h g^{-1}, corresponding to the extraction of 1.87 Li^+ ions per formula unit and a progressive discharge capacity of 234 mA h g^{-1}, related to 1.42 Li^+ ions per formula unit. The *Pmn21* phase of Li_2MnSiO_4 exhibits a plateau at 4.2 V, which is comparable with the value of Arroyo *et al*.,[28]corresponding to the first lithium extraction driven by Mn^{2+}/Mn^{3+} red-ox couple. However, the second plateau at 4.5 V, (observed upon extending cycling also) corresponds to the extraction of second lithium and hence responsible for the higher specific capacity values observed with respect to Li_2MnSiO_4/rGO cathode. i.e., stable charge/discharge capacity of about 210 mAh g^{-1} has been exhibited up to 100 cycles (Fig. 7) with 87% retention. More interestingly, the loss in capacity calculated for Li_2FeSiO_4/rGO and Li_2MnSiO_4/rGO cathodes after completing 100 cycles is found to be less than 15%. Therefore, it is clearly understood from this study that close to one lithium ion per formula from Li_2FeSiO_4/rGO and more than one lithium ion per formula from Li_2MnSiO_4/rGO cathode could be extracted/inserted from/into the composite matrix, which is the highlight of the study. Further, the charge-discharge behavior of Li_2MSiO_4/rGO composite cathodes (M=Fe, Mn) is definitely superior to the respective composites of orthosilicates obtained with 10 wt% CNT (Fig. 6a-b). With a view to gain more insights on the probable structural changes that favor the progressive cycling of Li_2MSiO_4/rGO (M=Fe, Mn) composite cathodes, ex situ XRD analysis has been made for the cells after completing few cycles i.e., XRD has been recorded for Li_2MSiO_4/rGO cathodes (M=Fe, Mn) after completing 5 cycles. To gain more understanding, we have recorded the XRD pattern after completing one cycle also (Fig. S11). As expected, significant change in the crystallinity (low intensity peaks) has been observed for both Li_2MnSiO_4/rGO and Li_2FeSiO_4/rGO cathodes after the completion of one cycle along with the formation of thermodynamically stable phases, as

reported in the literature[32,33]. Interestingly, the thus formed-thermodynamically favored structure of the respective composite is found to get maintained especially after 5 cycles, which in turn justifies the prolonged cycling stability of title cathodes upon extended cycles.

Electrochemical impedance spectroscopy was carried out to shed more light on the role of carbon additive in improving the electrochemical behavior. Fig.S12 represents the impedance behavior of individual Li_2MSiO_4/C (M=Fe, Mn) electrodes after first cycle and after completing 10 cycles. The corresponding Nyquist graphs are presented in Fig. S12, fitted with an equivalent circuit model. The intercept at the Z real axis in the high frequency refers to R_s, which includes electrolyte solution resistance and contact resistance. The semi-circle in the high and middle frequency range is due to the charge transfer resistance (R_{ct}); and the sloping line in the lower frequency represents lithium-ion diffusion resistance in electrode bulk, namely the Warburg impedance. It is evident from Fig. S12 that the R_{ct} value of Li_2MSiO_4/rGO is lower than those of the corresponding Li_2MSiO_4/CNT (M=Fe, Mn) composite cathodes, irrespective of the cycle number. Such a lower R_{ct} value exhibited by Li_2MSiO_4/rGO composites could be understood in terms of the appreciable conductivity of native rGO and the same has been further substantiated by the room temperature conductivity values measured for Li_2MSiO_4/rGO composites in comparison with M= Fe, Mn (Fig. S13), i.e., the room temperature conductivity values follow the order of Li_2MSiO_4 <Li_2MSiO_4/CNT< Li_2MSiO_4/rGO composites. More interestingly, the R_{ct} value of Li_2FeSiO_4/rGO and Li_2MnSiO_4/rGO cathodes decrease upon extended cycling, especially due to the gradual percolation of electrolyte, as discussed in the previous report.[31]Hence, the role of rGO by virtue of its inherent conductivity advantages in improving the ultimate conductivity as well as the electrochemical lithiation and de-lithiation of resultant

Li_2MSiO_4/rGO (M=Fe, Mn) composite cathodes by facilitating facile lithium-ion transport could be understood.

Further, the effect of rGO in offering facile lithium diffusion kinetics upon different current rates has been investigated by subjecting the cells (containing Li_2MSiO_4/rGO cathodes) individually to C/2, C/10 and C/20 rates (Fig. 7), after completing 100 cycles at C/20 rate. Despite the completion of 100 cycles, Li_2MnSiO_4/rGO composite cathode exhibits reasonable capacity values of 142 mAh g^{-1} (C/10) and 95 mAh g^{-1} (C/2) upon extended cycling, which is superior than the reported capacity values.[35,36] On the other hand, Li_2FeSiO_4/rGO composite cathode shows slightly inferior capacity values of 98 mAh g^{-1} (C/10) and 53mAh g^{-1} (C/2) under similar conditions, thus recommending Li_2MnSiO_4/rGO cathode as a potential candidate for rechargeable lithium battery applications.

4. Conclusion

Custom designed nano crystalline Li_2FeSiO_4/rGO and Li_2MnSiO_4/rGO composite cathodes have been demonstrated to deliver a steady state and room temperature specific capacity of 149 and 210 mAh g^{-1} with less than 15% fade in capacity up to 100 cycles. A low temperature solvothermal synthesis is found to be suitable to prepare such nanocrystalline composite cathodes in the desired phase with high capacity behavior in preference with the conventionally adopted sol-gel method. Similarly, reduced graphene oxide (rGO) is found to be effective in exhibiting superior electrochemical behavior of orthosilicate cathodes of the present study compared with CNT, especially when prepared in the form of Li_2MSiO_4/rGO (M=Fe, Mn) composite cathodes. rGO with its inherent appreciable conductivity promotes lithium diffusion kinetics and the coverage of Li_2MSiO_4 surface with rGO offers better protection against parasitic side reactions, thus responsible for the excellent electrochemical behavior. Particularly,

Li_2MnSiO_4/rGO cathode is recommended as a high capacity electrode material with superior discharge capacity values.

Acknowledgements

Among the authors, D. Bhuvaneswari is thankful to the Council of Scientific and Industrial Research (CSIR), India for financial support through Senior Research Fellowship and N. Kalaiselvi to CSIR for financial support through MULTIFUN Project.

References

1. J. B. Goodenough, H. Y. P. Hong, J. A. Kafalas, *Mater. Res. Bull*., 1976, **11**, 203.
2. A. K. Padhi, K. S. Nanjundaswamy, C. Masquelier, S. Okada, J. B. Goodenough, *J. Electrochem.Soc*., 1997, **144**, 1609.
3. J. B. Goodenough, Y. J. Kim, *J. Power Sources*, 2011, **196**, 6688.
4. A. Nyten, A. Abouimrane, M. Armand, T. Gustafsson, J. O. Thomas, *Electrochem. Commun*., 2005, **7**, 156.
5. Z. Chen, S. Qiu, Y. Cao, J. Qian, X. Ai, K. Xie, X. Hong, H. Yang, *J. Mater. Chem. A*, 2013, **1**, 4988.
6. D. M. Kempaiah, D. Rangappa, I. Honma, *Chem. Commun*., 2012, **48**, 2698.
7. A. Nyten, M. Stjerndahl, H. Rensmo, H. Siegbahn, M. Armand, T.Gustafsson, K. Edstrom, J. O. Thomas, *J. Mater. Chem.,* 2006, **16**, 3483.
8. K. Zaghib, A. A. Salah, N. Ravet, A. Mauger, F. Gendron, C. M. Julien, *J. Power Sources*, 2006, **160**, 1381.
9. M. S. Islam, R. Dominko, C. Masquelier, C. Sirisopanaporn, A. R. Armstrong, P. G. Bruce, *J. Mater. Chem.,*2011, **21**,9811.
10. B. L. Ellis, K. T. Lee, L. F. Nazar, *Chem. Mater*., 2010, **22**, 691.

11. A. R. Armstrong, N. Kuganathan, M. S. Islam, P. G. Bruce, *J. Am. Chem. Soc.*, 2011, **133**, 13031.

12. S. I. Nishimura, S. Hayase, R. Kanno, M. Yashima, N. Nakayama, A. Yamada, *J. Am. Chem., Soc*. 2008, **130**, 13212.

13. T. Muraliganth, K. R. Stroukoff, A. Manthiram, *Chem. Mater*., 2010, **22**,5754.

14. M. E. Arroyo-de Dompablo, M. Armand, J. M. Tarascon, U. Amador, *Electrochem. Commun*., 2006, **8**,1292.

15 C. Deng, S. Zhang, B. L. Fu, S. Y. Yang, L. Ma, *Mater. Chem. Phys*., 2010, **120**,14.

16. R. Dominko, M. Bele, M. Gaberscek , A. Meden, M. Remskar, J. Jamnik, *Electrochem. Commun.,* 2006, **8**, 217.

17. A. Peigney, C. Laurent, E. Flahaut, R. R. Bacsa, Rousset, *Carbon*, 2001, **39**, 507.

18. D. R. Dreyer, S. Park, C. W. Bielawski, R. S. Ruoff, *Chem. Soc. Rev*., 2010, **39**, 228.

19. Y. Shi, S. -L. Chou, J. -Z. Hao Wang, D. Wexler, H. -J. Li, H. -K. Liu, Y. Wu, *J. Mater. Chem.*, 2012, **22**, 16465.

20. Y. Tang, F. Huang, H. Bi, Z. Liu, D. Wan, *J. Power Sources*, 2012, **203,** 130.

21. Gerard Demazeau, *J. Mater. Chem*. 1999, **9**, 15.

22. D. Cruz, S. Bulbulian, *J. Am. Ceram. Soc*., 2005, **88**, 1720.

23. A. C. Ferrari, J. C. Meyer, V. Scardaci, C. Casiraghi, *Phys. Rev. Lett*., 2006, **97**, 187401.

24. W. Gao, L. B. Alemany, L. Ci, P. M. Ajayan, *Nat. Chem*., 2009, **1**, 403.

25. E. Strauss, G. Ardel, V. Livshits, L. Burstein, D. Golodnitsky, E. Peled, *J. Power Sources*, 2000, **88**, 206.

26. B. Shao, Y. Abe, I. Taniguchi, *Powder Technol*., 2013, **235**, 1.

27. A. R. Armstrong, N. Kuganathan, M. S. Islam, P. G. Bruce, *J. Am. Chem. Soc*., 2011, **133**,

13031.

28. M. E. Arroyo-de Dompablo, M. Armand, J. M. Tarascon, U. Amador, *Electrochem. Commun.,* 2006, **8**, 1292.

29. D. M. Kempaiah, D. Rangappa, I. Honma, *J. Mater. Chem*., 2012, **22**,12128.

30. D. Lu, W. Wen, X. Huang, J. Bai, J. Mi, S. Wu,Y. Yang, *J. Mater. Chem.,* 2011, **21**, 9506.

31. A. J. Bard, J. R. Faulkner, *Electrochemical Methods*, second ed., Wiley, 2001, p 231.

32. Yi Zhao, Jiaxin Li, Ning Wang, Chuxin Wu, Yunhai Ding, Lunhui Guan, J. Mater. Chem., 2012, **22**, 18797.

33. S. Devaraj, M. Kuezma, C. T. Ng, P. Balaya, Electrochimica Acta, 2013, **102** , 290.

34. H. Gong, Y. Zhu, L. Wang , D. Wei, J. Liang, Y. Qian, *J. Power Sources*, 2014, **246**, 192.

35. L. Qu, S. Fang, L. Yang, S. Hirano, *J. Power Sources,* 2014, **252**, 169.

Figures

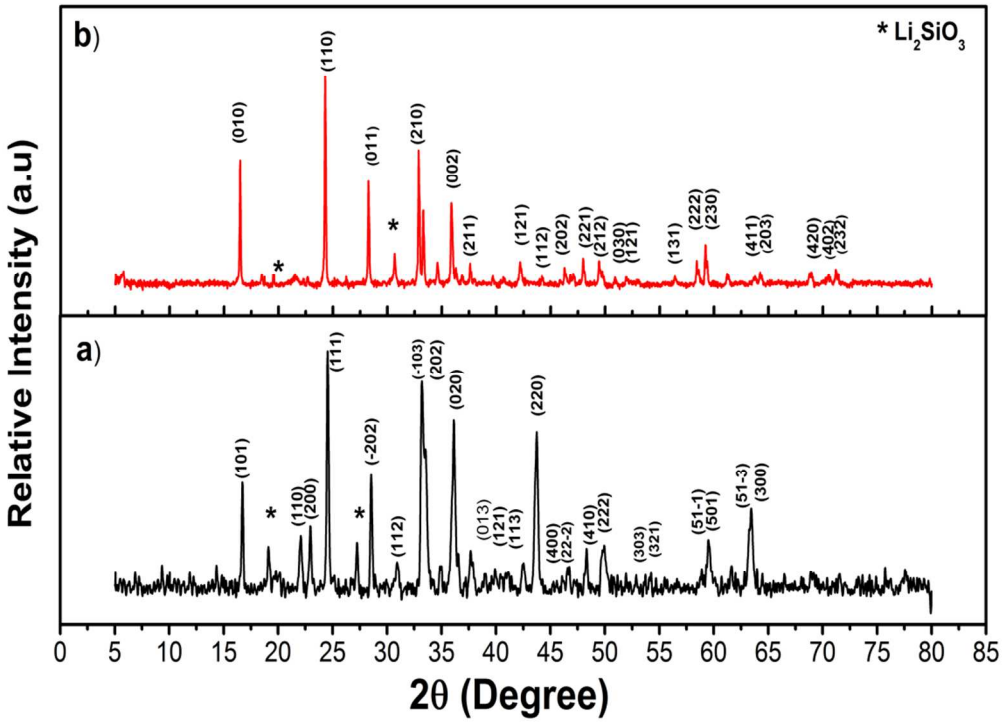

Fig. 1 XRD pattern of (a) Li_2FeSiO_4/rGO and (b) Li_2MnSiO_4/rGO samples synthesized by solvothermal process at 300°C

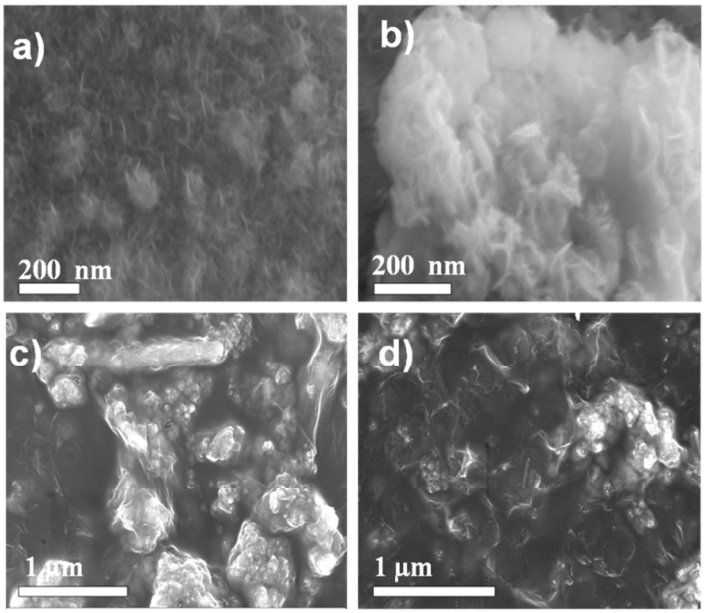

Fig. 2 FESEM images of (a-b) Li_2FeSiO_4/rGO; (c-d) Li_2MnSiO_4/rGO

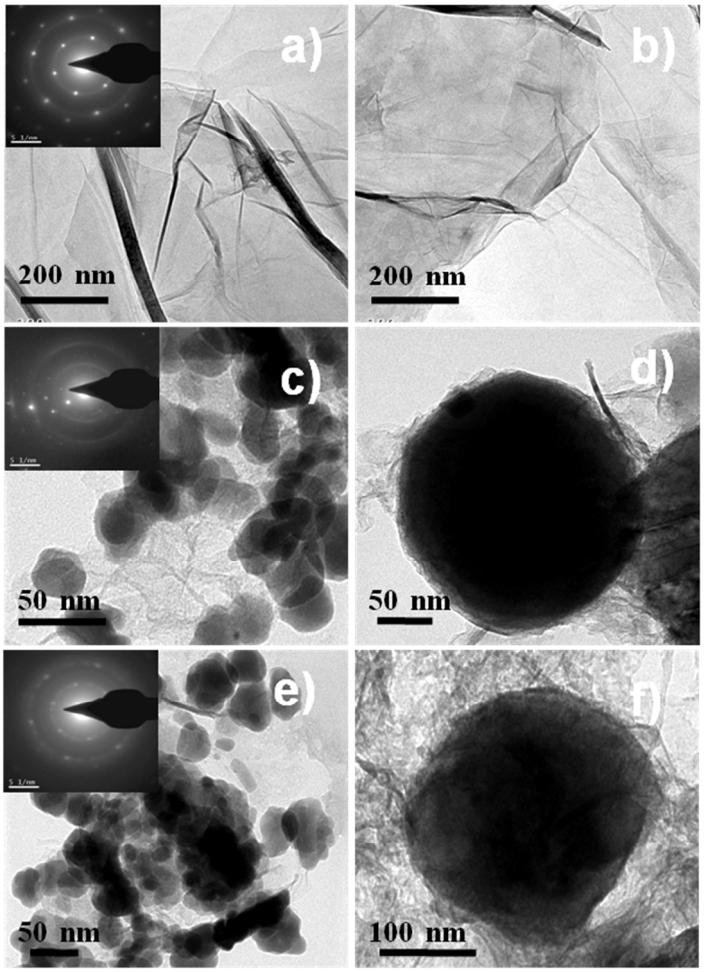

Fig. 3 TEM images of (a-b) transparent rGO sheet and Inset: SAED pattern of rGO; (c-d) Li_2FeSiO_4/rGO sample and Inset: SAED pattern of Li_2FeSiO_4/rGO; (e-f) Li_2MnSiO_4/rGO sample and Inset: SAED pattern of Li_2MnSiO_4/rGO composite

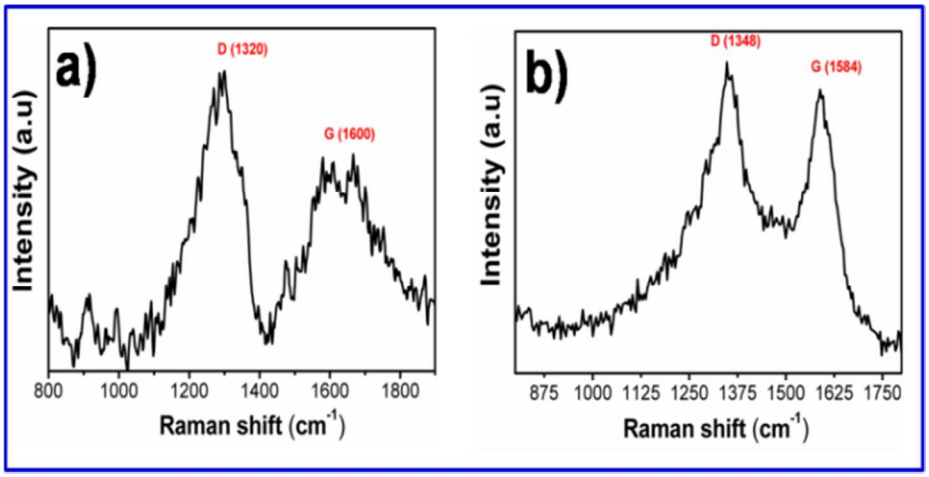

Fig. 4 Raman spectrum of (c) Li_2FeSiO_4/rGO and (d) Li_2MnSiO_4/rGO composites

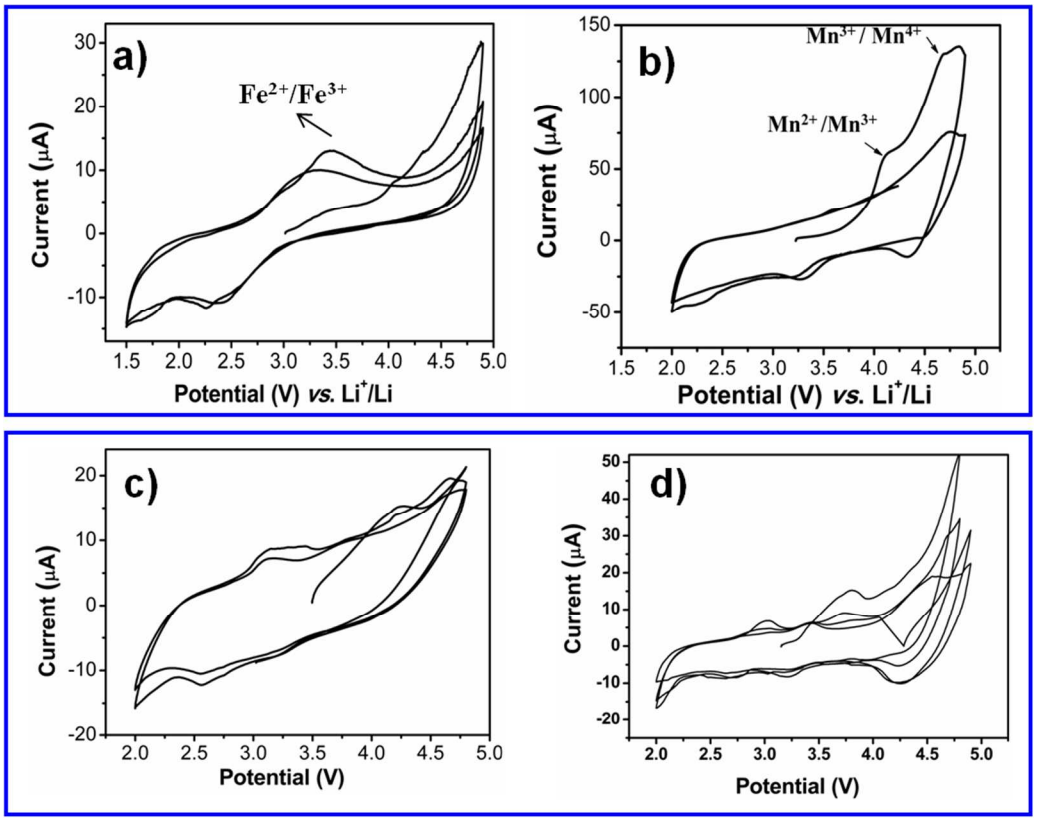

Fig. 5 Cyclic voltammogram of Li_2MSiO_4/C composite cathode measured at room temperature vs. Li/Li^+; (a) Li_2FeSiO_4/rGO and (b) Li_2MnSiO_4/rGO (c) Li_2FeSiO_4/CNT and (d) Li_2MnSiO_4/CNT

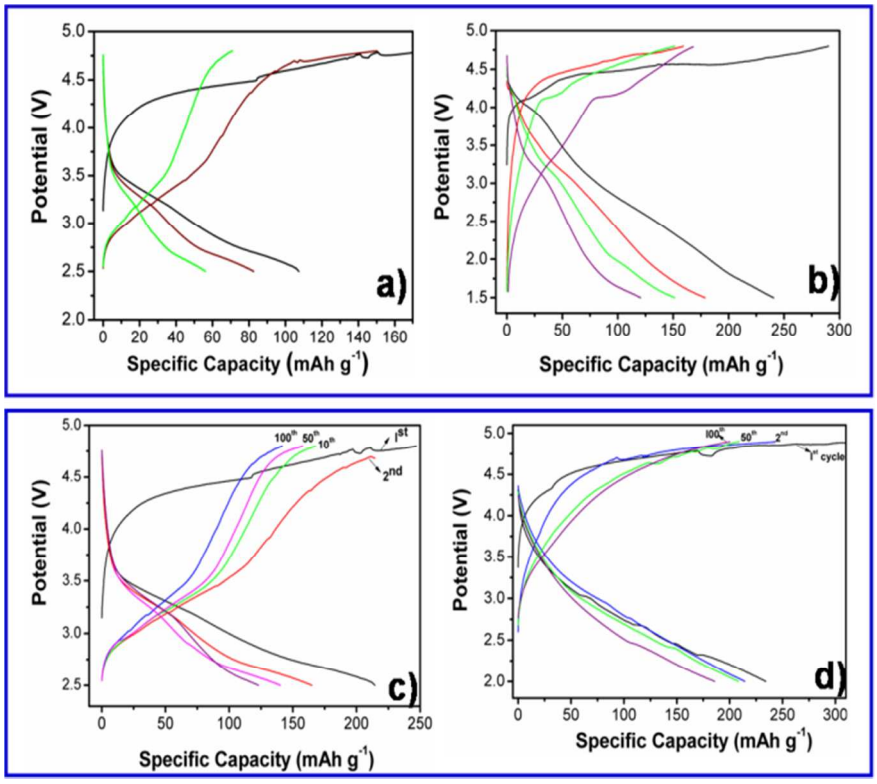

Fig. 6 Charge-discharge profile of Li_2MSiO_4/C composite cathode at a current rate of C/20 (a) Li_2FeSiO_4/CNT (b) Li_2MnSiO_4/CNT (c) Li_2FeSiO_4/rGO and (d) Li_2MnSiO_4/rGO

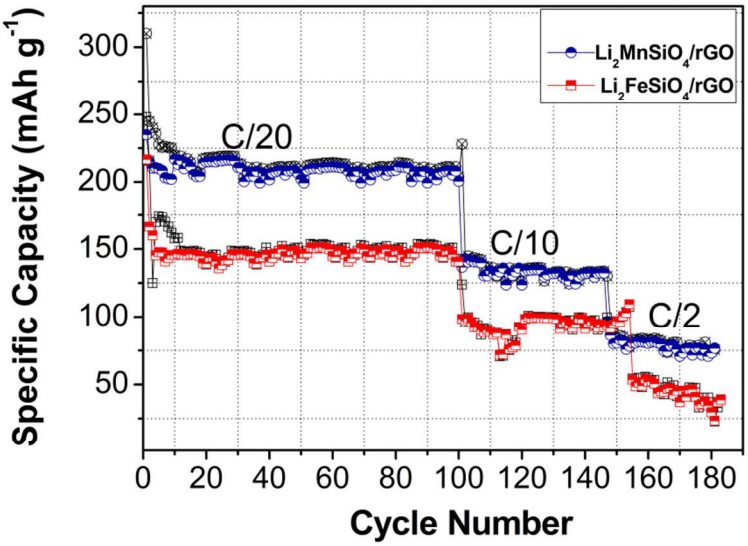

Fig. 7 Cycling performance of Li_2FeSiO_4/rGO and Li_2MnSiO_4/rGO cathodes at different current rates